Electromagnetics, 32:481–494, 2012
Copyright © Taylor & Francis Group, LLC
ISSN: 0272-6343 print/1532-527X online
DOI: 10.1080/02726343.2012.726914

Taylor & Francis
Taylor & Francis Group

Low-Profile Automotive Antenna for Omnidirectional Vertical Polarized Signal Reception

SEUNGHEE BAEK[1] and SUNGJOON LIM[1]

[1]Department of Electrical and Electronics Engineering, School of Engineering, Chung-Ang University, Seoul, Republic of Korea

Abstract *A low-profile antenna is designed for a WiBro vertical polarized signal. The proposed antenna is packaged and installed on the roof of a vehicle. The low-profile configuration is inspired from a zero-phase constant that realizes a horizontal magnetic loop current distribution equivalent to a vertical electric current distribution. With the proposed antenna, a wide bandwidth is achieved by overcoming the narrow bandwidth characteristics of an antenna with a zero-phase constant. The antenna was designed using a large conductive plate to simulate the vehicle roof in the electromagnetic simulation, thereby dramatically reducing simulation time. The results are comparable to the experimental results of an antenna on a vehicle's roof. The unpackaged and packaged antennas' radiation patterns are first measured in an anechoic chamber. Azimuth patterns are measured by installing the packaged antenna on the vehicle's roof. Simulations agree with experimental data where the vertically polarized signal is successfully received with a reasonable gain and efficiency in a WiBro band.*

Keywords small antenna, zeroth-order resonant antenna, metamaterial, spiral-slotted ground

1. Introduction

In automotive communication systems, reliable, cheap, and simply manufactured automotive antennas are required. An important design consideration is determining where to mount the antenna to receive the best signal. Much automotive antenna research (Iizuka et al., 2005; Zhang et al., 2009; Funato et al., 2009; Leng et al., 2007; Gschwendtner & Wiesbeck, 2003) has been conducted, referring to various mounted positions, such as on windows (Iizuka et al., 2005; Zhang et al., 2009; Funato et al., 2009), wheels (Leng et al., 2007), the bodyworks (Gschwendtner & Wiesbeck, 2003), and the roof. An automotive antenna was mounted for digital terrestrial reception on the top of the front and rear windows in Iizuka et al. (2005). In Zhang et al. (2009), the way in which

Received 30 March 2012; accepted 31 August 2012.
Address correspondence to Sungjoon Lim, #534 Bobst Hall, Department of Electrical and Electronics Engineering, School of Engineering, Chung-Ang University, 221, Hukseok-dong, Dongjak-gu, Seoul, 156-756, Republic of Korea. E-mail: sungjoon@cau.ac.kr

vehicle equipment affects performance of a window-mounted antenna was investigated. Electromagnetic simulation results for a GPS antenna mounted on the front windshield were presented in Funato et al. (2009). Wheel and rear bodyworks were proposed as mounted positions of automotive antennas in Leng et al. (2007) and Gschwendtner and Wiesbeck (2003), respectively. The roof is an especially good place to mount the antenna. Many roof-mounted automotive antennas, such as a monopole antennas, PIFA (planar inverted-F antenna), and PCB (printed circuit board) antennas, were proposed in Hansen and Hofmann (2008), Leelaratne and Langley (2005), and Walbeoff and Langley (2005), respectively. However, these protruding antennas can easily be damaged by environmental conditions, and they can spoil the car's profile in terms of exterior beauty. Therefore, a low-profile antenna, such as a hidden antenna mounted on the roof of a car, is greatly desirable (Low et al., 2006). A low-profile antenna can easily be designed for satellite communications (Hui et al., 2004; Chen et al., 2011; Saed & Yadla, 2006) because of horizontal polarization. In contrast, it is difficult to implement low-profile antennas with vertical polarized signal reception for terrestrial services. Several approaches receive a vertically polarized wave on a low-profile aperture. The zero-phase constant (Qureshi et al., 2005; Antoniades & Eleftheriades, 2008; Hwang et al., 2009), surface wave (Yang et al., 2007), or small magnetic loop (Hong & Sarabandi, 2008) can be applied for these requirements. A metamaterial ring antenna with a height of 6.8 mm ($\lambda 0/28$) produces a vertical polarized electric current distribution (Qureshi et al., 2005). Two vertical vias become in-phase because of the zero insertion phase between them. However, the metamaterial ring antenna needs a quarter-wavelength sleeve balun. In Antoniades and Eleftheriades (2008), a metamaterial-based folded monopole antenna was proposed with a height of 5 mm ($\lambda 0/20$), vertical electric field polarization, and narrow bandwidth. As an alternative, it is thought that the surface wave antenna can receive a vertical polarized signal (Yang et al., 2007). A surface wave antenna is composed of a thin grounded dielectric slab with a periodic patch, and it is excited by the circular patch. Surface wave diffraction at the slab produces vertical polarization, and the antenna has only a 3-mm ($0.05\lambda 0$) thickness. In Hong and Sarabandi (2008), vertical polarization was achieved by using a small magnetic loop, since the magnetic loop is equivalent to an electric dipole. Its configuration consists of a slot loop and a cavity under the slot loop.

In this article, a low-profile roof-mounted automotive antenna is proposed for vertical polarized signal reception. The metamaterial structure is introduced to receive a vertical polarized electric field on the low-profile aperture. Its unique zeroth-order resonance phenomenon realizes an efficient magnetic loop current distribution that generates equivalently vertical electric field distributions while yielding a narrow bandwidth. The proposed low-profile antenna has a wide bandwidth that is due to a novel circular patch structure and an increased thickness. Since the proposed low-profile antenna is installed on the roof of the vehicle, the car body effects are studied by modeling, using a large conductive plate in the simulation environment. Its network and radiation performances are experimentally investigated in an anechoic chamber, as well as outdoors in the field. The packaging issues are considered, and the antenna's mounting positions are optimized from the field test.

This article is organized as follows: in Section 2, a way to realize the low-profile antenna is discussed. In Section 3, the proposed low-profile antenna is applied to an automotive antenna, and several considerations are discussed for vehicle applications. In addition, the packaging issue and field test are stated. Their numerical and experimental results are compared and discussed. Finally, conclusions are drawn in Section 4.

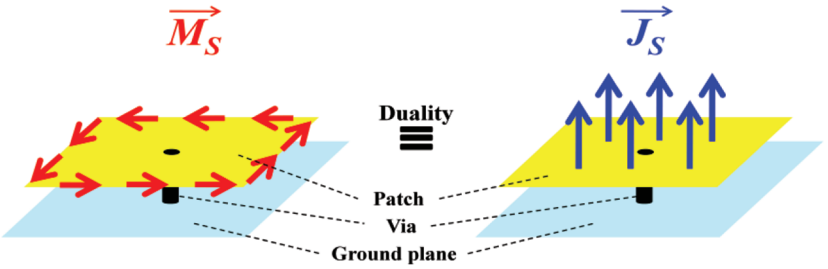

Figure 1. Duality relationship between the horizontal magnetic current distributions ($\vec{M}_s$) and the vertical electric current distributions ($\vec{J}_s$). (color figure available online)

2. Low-Profile Antenna Design

2.1. ZOR Phenomenon

To realize a low-profile antenna with vertical polarization, the concept of a zero-phase constant is used (Lai et al., 2007). If a zero-phase constant is incurred at a specific frequency, the infinite wavelength is obtained from

$$\beta = \frac{2\pi}{\lambda}, \tag{1}$$

where β is a phase constant, and λ is a wavelength. Because of the infinite wavelength, a constant magnetic current flows around the patch so that a vertical polarization can be produced at a planar antenna. It is well-known from the duality theorem that the vertical electric current distribution is equivalent to the horizontal magnetic current distribution and vice versa (Stutzman & Thiele, 1998). The proposed low-profile antenna design is based on Sievenpiper's mushroom structure (Sievenpiper et al., 1999). Figure 1 shows a duality relation between the horizontal magnetic current distributions ($\vec{M}_s$) and the vertical electric current distributions ($\vec{J}_s$) on the square mushroom structure. Since the magnetic current loop has a constant phase around the patch, it becomes equivalent to the vertical electric current. A zero-phase constant is produced by realizing a periodic composite right-/left-handed transmission line (CRLH TL) (Caloz & Itoh, 2005; Yu et al., 2008; Baek & Lim, 2009). Figure 2(a) displays the equivalent circuit model of a unit cell

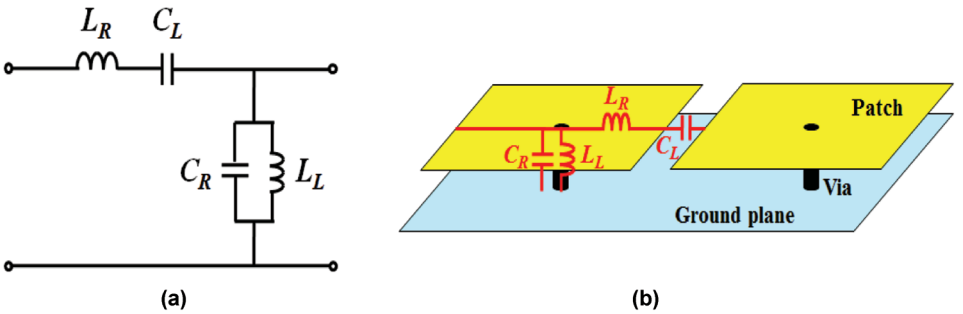

Figure 2. CRLH TLs: (a) equivalent circuit model of a unit-cell and (b) mushroom structure with two unit cells. (color figure available online)

of CRLH TL that is composed of the series inductance (L_R)/capacitance (C_L) and the shunt inductance (L_L)/capacitance (C_R), where the specific resonance with a zero-phase constant occurs that is due to L_L and C_R. CRLH TLs with two unit-cells are illustrated in Figure 2(b).

From the periodic boundary conditions and the Bloch–Floquet theorem, the phase constant of the CRLH unit cells is given by

$$\beta = \frac{2\pi}{d}\cos^{-1}\left(1 - \frac{1}{2}\left(\frac{\omega_L^2}{\omega^2} + \frac{\omega^2}{\omega_R^2} - \frac{\omega_L^2}{\omega_{se}^2} - \frac{\omega_L^2}{\omega_{sh}^2}\right)\right), \tag{2}$$

where

$$\begin{aligned} \omega_L &= \frac{1}{\sqrt{C_L L_L}}, \qquad & \omega_R &= \frac{1}{\sqrt{C_R L_R}}, \\ \omega_{se} &= \frac{1}{\sqrt{C_L L_R}}, \qquad & \omega_{sh} &= \frac{1}{\sqrt{C_R L_L}}. \end{aligned} \tag{3}$$

From Eq. (2), the phase constant becomes zero at ω_{se} and ω_{sh}. In the case of the open boundary condition, the zeroth-order resonant frequency is determined by the shunt resonant frequency (ω_{sh}). It is noticed from Eq. (3) that these frequencies are determined by circuit parameters.

The series inductance and the shunt capacitance are attributed to the microstrip patch, and the shunt inductance is due to the via. Moreover, the series capacitance is represented by the gap between the unit cells. The resonant frequency with the zero-phase constant is determined by controlling the overall physical components, such as the patch size, via length and radius, and dielectric constant. In addition, the substrate permittivity, loss tangent, thickness, and via size greatly affect the bandwidth and efficiency of the CRLH TL based antenna (Lai et al., 2007). Low tangential loss and big via radius improve the efficiency of the antenna with a zero-phase constant; while the bandwidth is increased because of the large thickness and low permittivity.

2.2. Antenna Design

Figure 3 illustrates the configuration of the proposed low-profile antenna with vertical polarization. The fan-shaped unit cells are introduced, where the equivalent circuit model of each unit-cell consists of series inductance (L_R)/capacitance (C_L) and shunt inductance (L_L)/capacitance (C_R). The unit cells have circular patch configurations rather than the generally square or rectangular patches since the circular patches slightly increase the bandwidth. To satisfy the bandwidth requirements for Korean WiBro service (2.3–2.4 GHz), the bandwidth is greatly increased because of the use of the multilayer substrates (i.e., subs 1, 2, and 3 as shown in Figure 3). In order to employ the proposed antenna commercially, the cost is considered, and thus, the FR4 substrates with a permittivity of 4.4 and a thickness of 1.6 mm are used for subs 1 and 3. Foam substrate with a permittivity of about 1 and a thickness of 5 mm is inserted between the sub 1 and 3. Once the permittivity and thickness of the substrate are determined, the proper-sized via radius is chosen for radiation efficiency, and the patch size is controlled for the designated frequency. The proposed antenna has a via radius of 0.4 mm. The rectangular patch at the feeding point is adjusted for impedance matching.

The generated zero-phase constant is numerically demonstrated through the electric field distributions, as shown in Figure 4, where the phase of a vertical polarized E-field

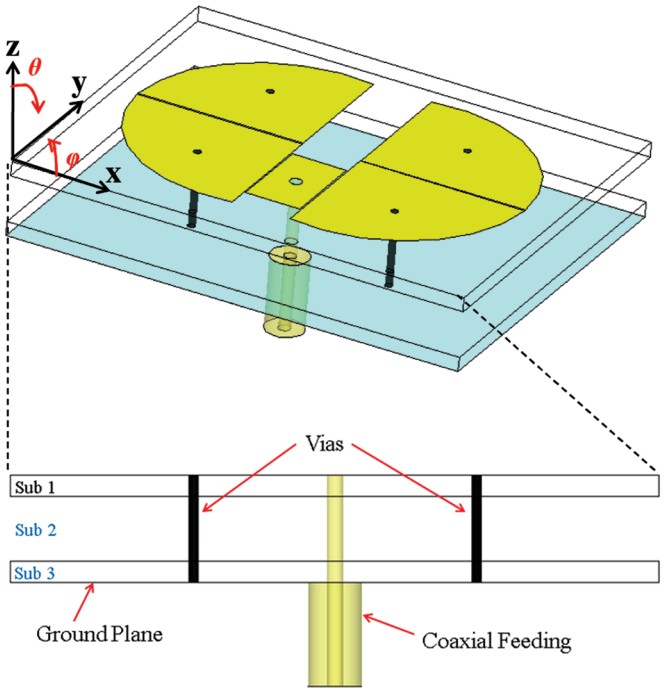

Figure 3. Configurations of the proposed low-profile antenna (subs 1 and 3: FR4, sub 2: foam). (color figure available online)

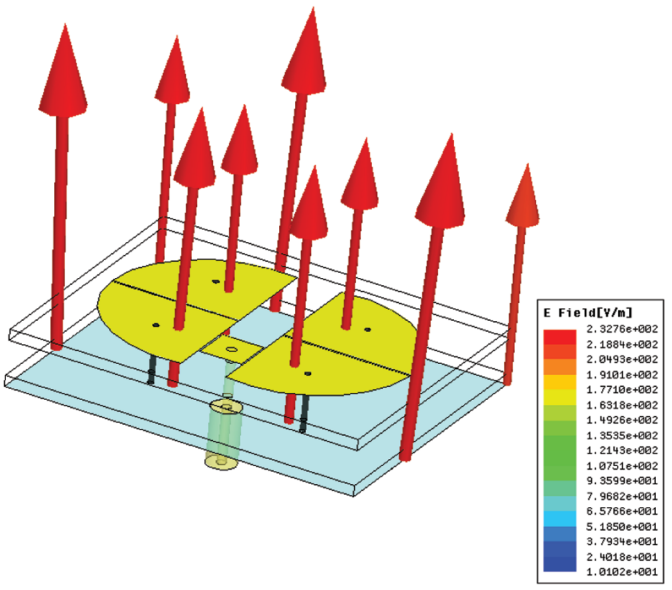

Figure 4. *E*-field vectors of the proposed low-profile antenna to demonstrate a zero phase constant. (color figure available online)

is not changed. Therefore, the proposed antenna can be considered as a good candidate for a roof-mounted automotive antenna receiving a vertically polarized signal.

3. Automotive Antenna Application

3.1. *Considerations for Automotive Antenna Application*

The mounting conditions on the vehicle need to be considered to implement the proposed low-profile antenna as an automotive antenna. A large conductive plate ($2.3\lambda0 \times 2.3\lambda0$) is used in the simulation environment as a substitute for the roof of a car. This reduces simulation time. Experimental results will be compared to verify that this simplified modeling is reasonable. The proposed antenna's performances are first investigated in an anechoic chamber, and then an outdoor field test is performed by installing the antenna on the roof of a mid-sized vehicle. Gain patterns are compared at three different positions on the roof. The impedance and radiation pattern variations are observed before and after packaging.

Figure 5 displays photographs of the fabricated antenna with the large conductive plate and the package. The proposed low-profile antenna is fabricated on two 1.6-mm FR4 substrate and 5-mm foam substrate, as shown in Figure 5(a). The fabricated low-profile antenna has an overall size of 40 mm (L_1) × 50 mm (W_1) × 8.2 mm (h_1) ($0.306\lambda0 \times 0.383\lambda0 \times 0.062\lambda0$ at 2.3 GHz). R_1 and R_2 of the fan-shaped patch exhibited

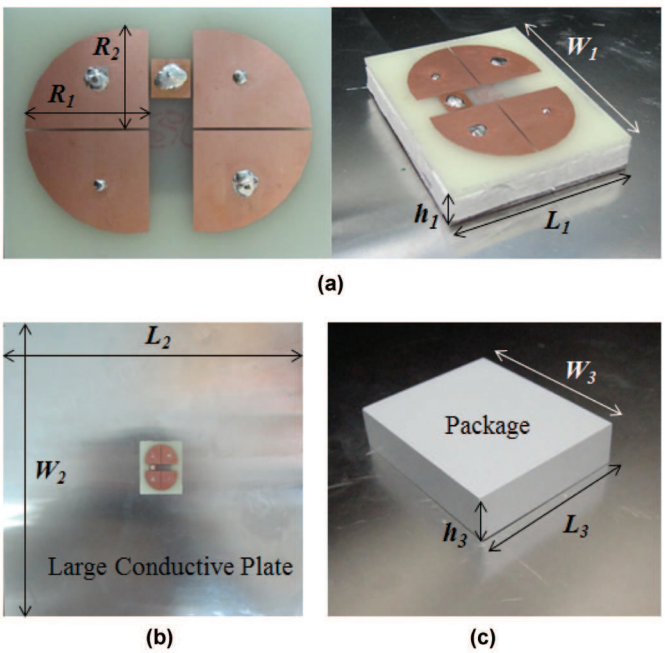

Figure 5. Photograph of the proposed low-profile vehicle antenna: (a) proposed antenna (R_1 = 18.2 mm, R_2 = 15 mm, L_1 = 40 mm, W_1 = 50 mm, h_1 = 8.2 mm), (b) with aluminum plate (L_2 = 300 mm, W_2 = 300 mm, h_2 = 1 mm), and (c) with package (L_3 = 50 mm, W_3 = 60 mm, h_3 = 14.5 mm). (color figure available online)

in Figure 3 are 18.2 mm and 15 mm, respectively. The gap between unit cells, as well as the gap between unit cells and the impedance matching patch, is 0.2 mm. The matching patch size is 6 mm × 6 mm. In Figure 5(b), the photo of the overall automotive antenna is shown, where the proposed antenna is positioned on the aluminium plate. The size of the aluminium plate is 300 mm (L_2) × 300 mm (W_2) × 1 mm (h_2). It is electrically $2.3\lambda0 \times 2.3\lambda0 \times 0.007\lambda0$. As shown in Figure 5(c), the antenna is packaged to protect it from environment conditions. Its exterior dimensions are 50 mm (L_3) × 60 mm (W_3) × 14.5 mm (h_3) ($0.383\lambda0 \times 0.460\lambda0 \times 0.111\lambda0$). Its interior dimensions are 45 mm × 55 mm × 12.5 mm. This package is made of acrylonitrile butadiene styrene (ABS) material, widely used for commercial automotive antennas, such as shark fin antennas. The package is simulated (and fabricated) with a permittivity of 2.32 and tangential loss of 0.0002.

3.2. Simulation and Measurement Results

The proposed low-profile automotive antenna is designed and simulated by using Ansoft's high-frequency structural simulator (HFSS; ANSYS, Canonsburg, Pennsylvania, USA). It is designed to have 10-dB bandwidth from 2.3 GHz to 2.4 GHz in the WiBro band. The 10-dB bandwidth for the proposed circular patch is 9.6% (2.19–2.41 GHz), which is an amount slightly higher than that of the square patch, which has 8.7% (2.2–2.4 GHz). In addition, the simulated efficiencies of the two different antennas are about 98% similar, and the simulated peak gains are 2.1 dBi for the proposed circular patch and 1.8 dBi for the square patch at 2.3 GHz in same conditions. In Figure 6, the simulated return loss of the proposed low-profile antenna without the large conductive plate is compared to that with the large conductive plate. When the large conductive plate is considered, its resonant frequency is decreased from 2.3 GHz to 2.16 GHz, and a slight impedance mismatch occurs. Therefore, the antenna is slightly modified to anticipate optimal performance in

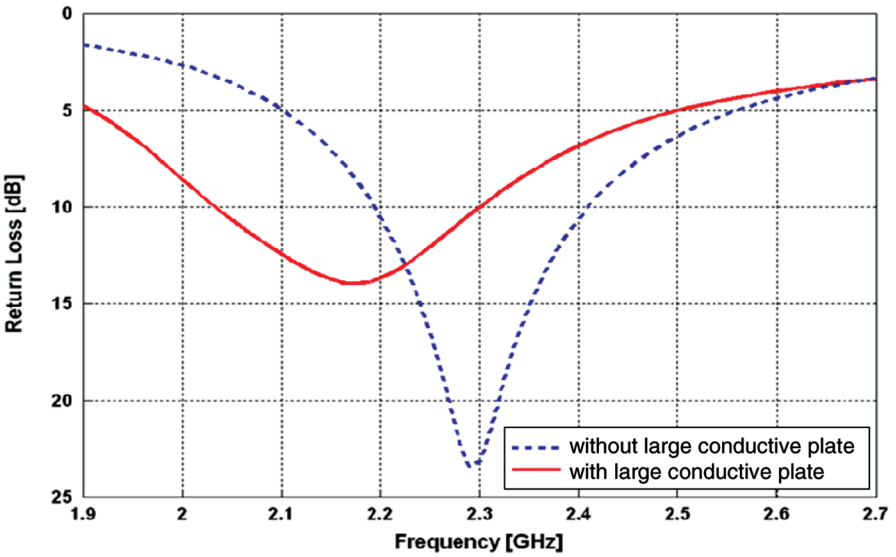

Figure 6. Simulated return losses with and without large conductive plate. (color figure available online)

the vehicle application. Figure 7 shows the return loss of the modified antenna with the large conductive plate. The modified antenna is compared with one after packaging. After packaging, its resonant frequency is decreased about 200 MHz. However, it still satisfies the WiBro band requirement. Before packaging, a return loss of 33 dB is obtained at 2.3 GHz, while a return loss of 16 dB at 2.1 GHz is obtained after the packaging antenna. The 10-dB bandwidth of the proposed automotive antenna with the package is calculated 18.2% (2–2.4 GHz). These measured results show slight deviations compared to the simulation results that are due to the experimental environment.

The proposed antenna's radiation characteristics are measured in an anechoic chamber. In Figures 8(a) to 8(d), simulated and measured gain patterns are plotted on the x-z- and x-y-planes. Each figure compares the packaged and unpackaged antennas' patterns while mounted on the large conductive plate. Figure 8(b) displays the measured gain patterns, with and without the package on the E-field (x-z-plane). Although the proposed antenna is packaged, a high peak gain of 4.5 dBi is obtained at 50°, and its radiation pattern remains the same as the unpackaged one. The $E\varphi$ level is measured -17 dBi at 50°. The measured H-field (x-y-plane) gain patterns with and without package are compared as well in Figure 8(d). After packaging, the gain of 3.5 dBi is observed at azimuth directions, and then the H_θ level of -18 dBi is obtained. All far-field simulation results are similar to the measured one, as shown in Figure 8. The far-field results verify that vertical signal reception is achieved at ± 50 elevation angles. Thus, the proposed automotive antenna can effectively receive a WiBro vertical polarized signal. In addition, it is shown that the proposed antenna is omnidirectionally radiating in the azimuth plane. In a 1.9- to 2.6-GHz band, the peak gains and efficiencies are simulated and measured with and without a package, as shown in Figures 9 and 10, respectively. The peak gain is greater than 4.5 dBi, and the radiation efficiency is higher than 67% in 1.9 to 2.6 GHz. The radiation efficiency is calculated by measuring the total radiation power in a three-dimensional radiation pattern.

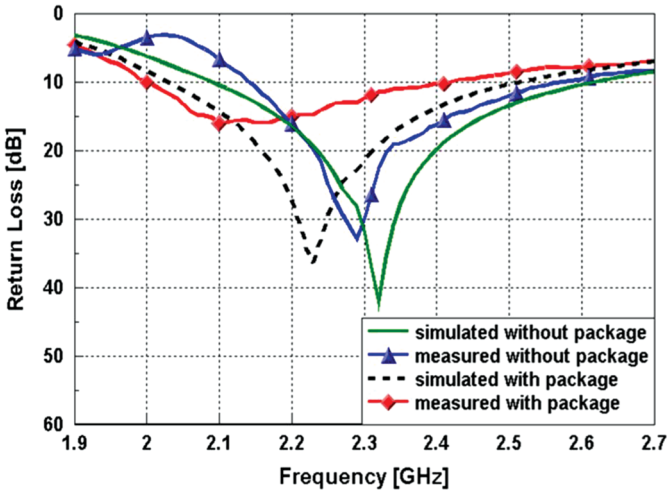

Figure 7. Simulated and measured return losses with and without package (with large conductive plate). (color figure available online)

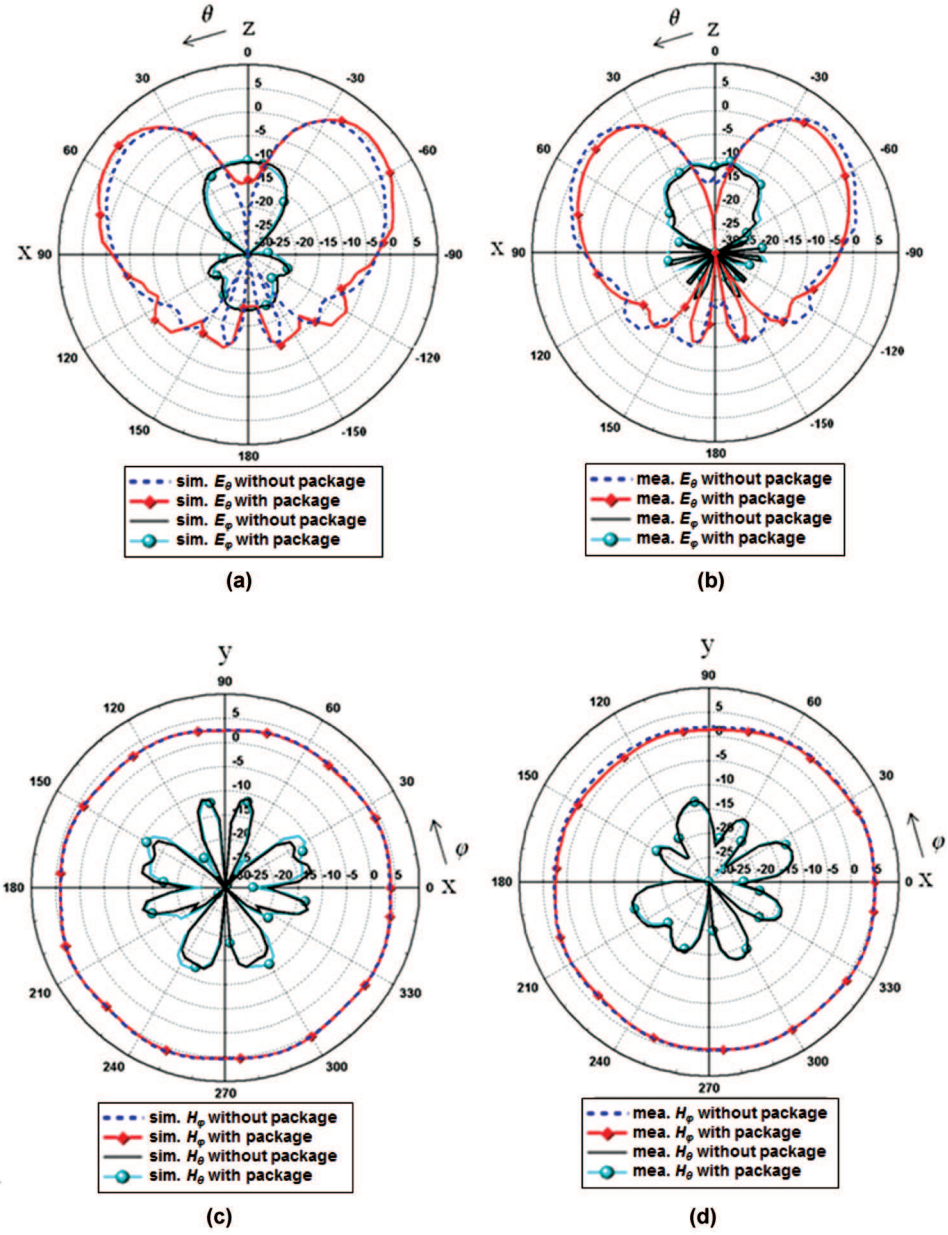

Figure 8. Simulated and measured gain patterns of proposed low-profile vehicle antenna with and without package at 2.3 GHz (unit: dBi): (a) simulated E_θ/E_φ, (b) measured $E_\theta/E\varphi$, (c) simulated H_φ/H_θ, and (d) measured H_φ/H_θ. (color figure available online)

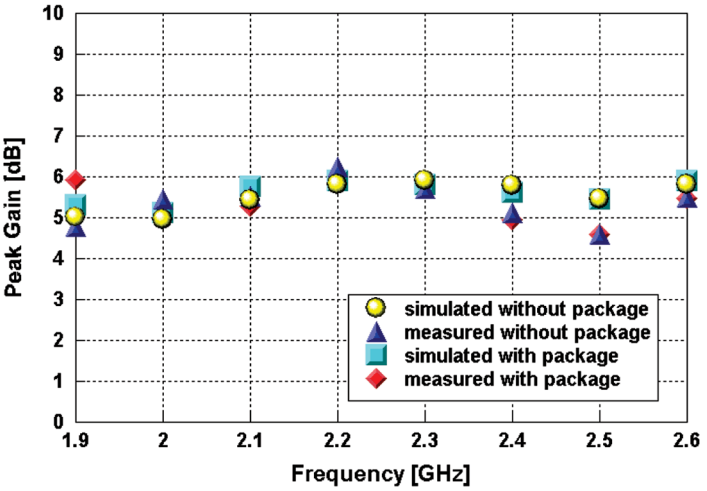

Figure 9. Simulated and measured peak gain with and without package. (color figure available online)

3.3. Field Test with Antenna on Vehicle's Roof

After simulating and measuring the proposed low-profile antenna with a large conductive plate, it is installed on the car's roof, and its radiation pattern is measured. Instead of the large conductive plate, the proposed antenna is mounted on the roof of a car. Moreover, the antenna is placed in three different positions. Each azimuth radiation pattern is measured and compared in the outdoor field-tests. Figure 11 shows a field-test setup where a mid-sized car is used and a radio frequency (RF) cable is inserted through the car's sunroof. The 2.3-GHz vertical polarized signal is transmitted by a

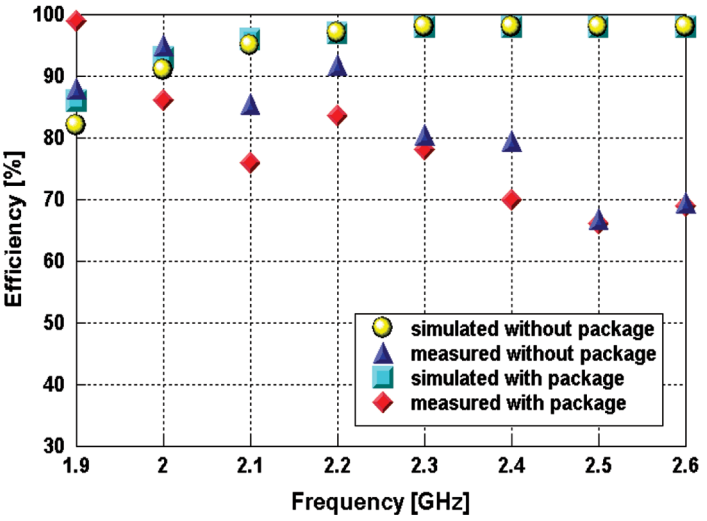

Figure 10. Simulated and measured efficiency with and without package. (color figure available online)

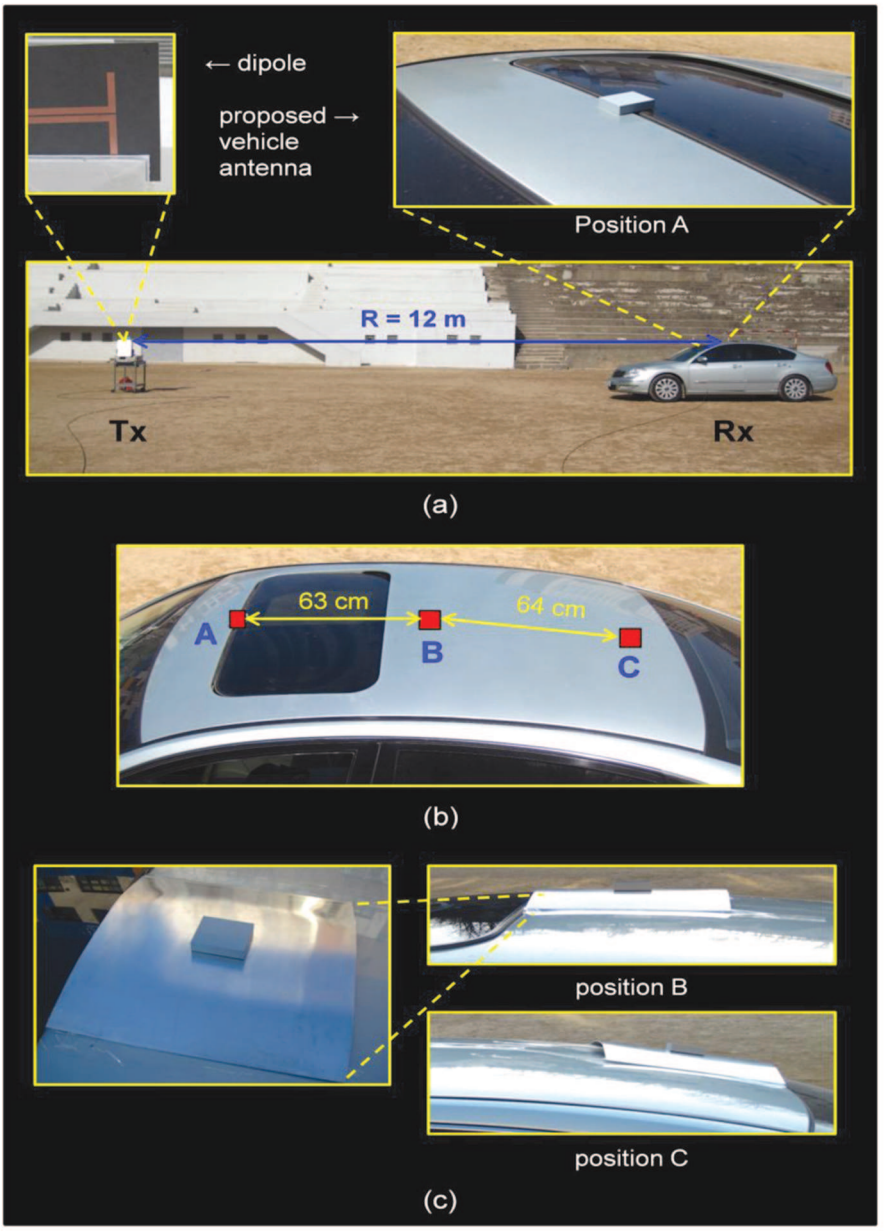

Figure 11. Photograph of field-test setup: (a) transmitter and receiver (position A); (b) positions A, B and C; and (c) photographs of proposed antenna mounted in positions B and C. (color figure available online)

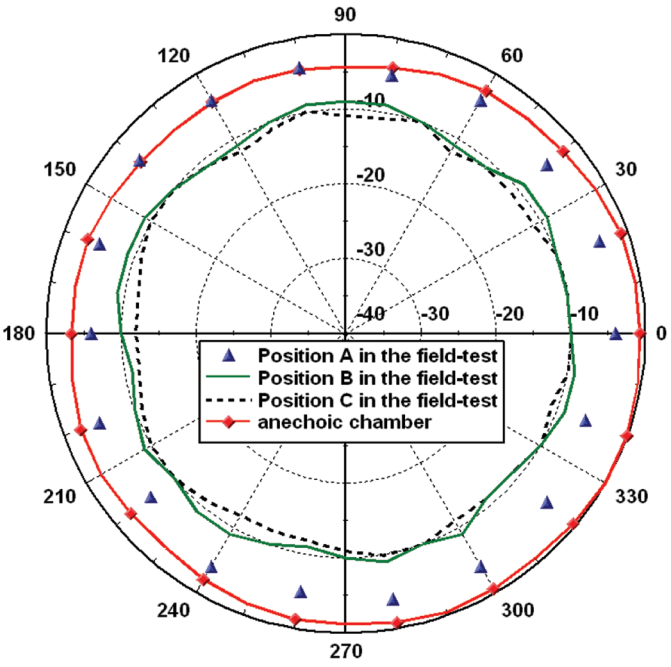

Figure 12. Measured radiation patterns of the proposed antenna at positions A, B, and C in the field-test as compared to that of the proposed antenna in an anechoic chamber. (color figure available online)

printed dipole antenna. The car is located 12 m from the transmitter, and the proposed antenna is used as a receiving antenna. The spectrum analyzer is left in the car to measure the received power. The mounted antenna and the spectrum analyzer are connected by slightly opening the sunroof, so that the RF cable can be inserted between them. The dipole antenna is rotated, and the test is repeated three times at positions A, B, and C, as shown in Figure 11(b). Distance R is varied to 12 m, 12.63 m, and 13.27 m at positions A, B, and C, respectively. Figure 12 shows the azimuth radiation patterns at each position. The proposed antenna has the highest gain at position A. From the radiation pattern on the elevation plane in Figure 8, the maximum intensity occurs at $\pm 50°$. As shown in Figure 11, the transmitting and receiving antennas are aligned in the same height, and positions A, B, and C are not on the flat plane. Thus, position A is the desired antenna installation position for the proposed antenna on the car used in this experiment. The optimized position can be different depending on a car's profile and the transmitting antenna positions. Nevertheless, in the present experiment, it is demonstrated that the results of vehicle field-tests are similar to the anechoic chamber results (Figure 8(d)) with the large conductive plate and without the vehicle; therefore, the antenna can be simulated on a large conductive plate instead of a huge car model, greatly reducing simulation time.

4. Conclusion

In this article, a low-profile packaged automotive antenna is proposed for omnidirectional vertical polarized signal reception. The proposed antenna supports a zero-phase constant using a metamaterial concept that realizes the vertical polarization despite its low-profile

configuration. In addition, it overcomes the narrow bandwidth property of metamaterial-based antennas. The radiation efficiency is greater than 70% in the WiBro band, and a peak gain of 5.7 dBi is obtained at 2.3 GHz. Even after packaging, the antenna with the commercial ABS material and its efficiency and gain degradation are all acceptable. This is verified from an anechoic chamber test showing that the vertical polarized signals are successfully received and that the maximum elevation angles occur at $\pm 50^{\circ}$. In addition, the outdoor test with the vehicle demonstrates that the proposed antenna is able to receive the vertical polarized signal omnidirectionally. In this article, although a single WiBro antenna is designed, it can easily be extended to multiple antennas because of the large amount of space on a vehicle's roof.

Acknowledgment

This work was supported by the National Research Foundation of Korea Grant funded by the Korean government (2009-0071958).

References

Antoniades, M. A., & G. V. Eleftheriades. 2008. A folded-monopole model for electrically small NRI-TL metamaterial antennas. *IEEE Antennas Wireless Propagat. Lett.* 7:425–428.

Baek, S., & S. Lim. 2009. Miniaturized zeroth-order antenna in spiral slotted ground plane. *IET Electron. Lett.* 45:1012–1014.

Caloz, C., & T. Itoh. 2005. Guided-wave applications. In *Electromagnetic metamaterials: Transmission line theory and microwave applications*, 1st ed. New Jersey: John Wiley & Sons.

Chen, A., T. Jiang, Z. Chen, & D. Su. 2011. A novel low-profile wideband UHF antenna. *Progr. Electromagn. Res.* 121:75–88.

Funato, H., H. Horita, S. Takaba, Y. Anzai, & M. Wisnewski. 2009. Electromagnetic simulation of on-glass antenna with vehicle body for telematics application. *IEEE Second European Wireless Technolgy Conference*, Rome, Italy, 28–29 September, 148–151.

Gschwendtner, E., & W. Wiesbeck. 2003. Ultra-broadband car antennas for communications and navigation applications. *IEEE Trans. Antennas Propagat.* 51:2020–2027.

Hansen, T., & F. Hofmann. 2008. Automotive multi- and broadband monopole antenna for GSM, WLAN, and UWB applications. *IEEE International Conference on Ultra-Wideband*, Hannover, Germany, 10–12 September, 219–222.

Hong, W., & K. Sarabandi. 2008. Low profile miniaturized planar antenna with omnidirectional vertically polarized radiation. *IEEE Trans. Antennas Propagat.* 56:1533–1540.

Hui, H. T., E. K. N. Yung, C. L. Law, Y. S. Koh, & W. L. Koh. 2004. Design of a small and low-profile 2×2 hemispherical helical antenna array for mobile satellite communications. *IEEE Trans. Antennas Propagat.* 52:346–348.

Hwang, R.-B., H.-W. Liu, & C.-Y. Chin. 2009. A metamaterial-based E-plane horn antenna. *Progr. Electromagn. Res.* 93:275–289.

Iizuka, H., T. Watanabe, K. Sato, & K. Nishikawa. 2005. Modified H-shaped antenna for automotive digital terrestrial reception. *IEEE Trans. Antennas Propagat.* 53:2542–2548.

Lai, A., K. M. K. H. Leong, & T. Itoh. 2007. Infinite wavelength resonant antennas with monopolar radiation pattern based on periodic structures. *IEEE Trans. Antennas Propagat.* 55:868–876.

Leelaratne, R., & R. Langley. 2005. Multiband PIFA vehicle telematics antennas. *IEEE Trans. Vehicular Tech.* 54:477–485.

Leng, Y., Q. Li, B. Hou, S. Liu, & T. Dong. 2007. Wheel antenna of wireless sensors in automotive tire pressure monitoring system. *IEEE International Conference on Wireless Communication, Networking and Mobile Computing*, Shanghai, China, 21–25 September, 2755–2758.

Low, L., R. Langley, R. Breden, & P. Callaghan. 2006. Hidden automotive antenna performance and simulation. *IEEE Trans. Antennas Propagat.* 54:3707–3712.

Qureshi, F., M. A. Antoniades, & G. V. Eleftheriades. 2005. A compact and low-profile metamaterial ring antenna with vertical polarization. *IEEE Antennas Wireless Propagat. Lett.* 4:333–336.

Saed, M., & R. Yadla. 2006. Microstrip-fed low profile and compact dielectric resonator antennas. *Progr. Electromagn. Res.* 56:151–162.

Sievenpiper, D., L. Zhang, R. F. J. Broas, N. G. Alexopolous, & E. Yablonovitch. 1999. High-impedance electromagnetic surfaces with a forbidden frequency band. *IEEE Trans. Microw. Theory Technol.* 47:2059–2074.

Stutzman, W. L., & G. A. Thiele. 1998. *Antenna theory and design*, 2nd ed., 68–71. New Jersey: John Wiley & Sons.

Walbeoff, A., & R. J. Langley. 2005. Multiband PCB antenna. *IEE Proc.-Microw. Antennas Propagat.* 152:471–475.

Yang, F., Y. Rahmat-Samii, & A. Kishk. 2007. Low-profile patch-fed surface wave antenna with a monopole-like radiation pattern. *IET Microw. Antennas Propagat.* 1:261–266.

Yu, A., F. Yang, & A. Elsherbeni. 2008. A dual band circularly polarized ring antenna based on composite right and left handed metamaterials. *Progr. Electromagn. Res.* 78:73–81.

Zhang, H., L. Low, J. Rigelsford, & R. Langley. 2009. Effects of vehicle furnishing on performance of aperture mounted multi-band conformal automotive antenna. *IEEE Third European Conference on Antennas and Propagation*, Berlin, Germany, 23–27 March, 2694–2697.

Copyright of Electromagnetics is the property of Taylor & Francis Ltd and its content may not be copied or emailed to multiple sites or posted to a listserv without the copyright holder's express written permission. However, users may print, download, or email articles for individual use.